Fungal Genetics and Biology 71 (2014) 21–31

Contents lists available at ScienceDirect

Fungal Genetics and Biology

journal homepage: www.elsevier.com/locate/yfgbi

The *Podosphaera xanthii* haustorium, the fungal Trojan horse of cucurbit-powdery mildew interactions

Jesús Martínez-Cruz [a], Diego Romero [a], José C. Dávila [b], Alejandro Pérez-García [a,*]

[a] *Instituto de Hortofruticultura Subtropical y Mediterránea "La Mayora", Universidad de Málaga, Consejo Superior de Investigaciones Científicas (IHSM-UMA-CSIC), Departamento de Microbiología, Facultad de Ciencias, Bulevar Louis Pasteur 31 (Campus de Teatinos), 29071 Málaga, Spain*

[b] *Departamento de Biología Celular, Genética y Fisiología, Facultad de Ciencias, Universidad de Málaga, Bulevar Louis Pasteur 31 (Campus Universitario de Teatinos), 29071 Málaga, Spain*

ARTICLE INFO

Article history:
Received 29 May 2014
Accepted 11 August 2014
Available online 20 August 2014

Keywords:
Callose
Haustorial lobes
Haustorium purification
Microscopy
Obligate biotrophy
Vesicles

ABSTRACT

The powdery mildew fungi are obligate biotrophic plant pathogens that develop a specialized structure for parasitism termed haustorium, which is responsible for nutrient uptake and factor exchange with the plant. In this work, we present a detailed microscopy analysis of the haustoria of the cucurbit powdery mildew fungus *Podosphaera xanthii*, a major limiting factor for cucurbit production worldwide. Despite being located inside plant epidermal cells, transmission electron microscopy (TEM) analysis showed the characteristic highly irregular outline of the extrahaustorial membrane that separates the extrahaustorial matrix of haustoria from the cytoplasm of the plant cell. TEM analysis also revealed the presence of some vesicles and electron-dense plaques of material surrounding the haustoria. In confocal microscopy analysis and aniline blue staining we found a positive correlation between haustorial development and deposition of callose, which is distributed as plaques around haustorial complex. In this study, a method for the isolation of *P. xanthii* haustoria was also adapted, which permitted the analysis of the formation of haustorial lobes and the visualization of vacuoles and the pool of vesicles inside the haustorial complex. Our findings suggested that the haustorial lobes were responsible for vesicular trafficking and most likely act as the main mediators of the fungus-plant dialogue. All of these findings were integrated into a model of the *P. xanthii*-host cellular interactions.

© 2014 Elsevier Inc. All rights reserved.

1. Introduction

Powdery mildews are probably the most common, conspicuous, widespread and easily recognizable plant diseases. Important crops, including cereals, grapevines and a number of vegetable and ornamental plants, are among their major targets (Agrios, 2005). Numerous vegetable crops are susceptible to powdery mildew, but cucurbits are arguably the most severely affected group (Pérez-García et al., 2009). In cucurbits, the disease can be caused by two fungal species, *Podosphaera xanthii* (synonym *Podosphaera fusca*) and *Golovinomyces orontii* (synonym *Golovinomyces cichoracearum*), which induce the following identical symptoms: off-white, talcum-like, powdery fungal growths that develop on both leaf surfaces, petioles and stems and sometimes on fruits (Pérez-García et al., 2009). The two species, however, can be easily distinguished from one another using light microscopy; *P. xanthii* conidia are ovoid-shaped, germinate laterally and contain refractive crystals known as fibrosin bodies, whereas *G. orontii* conidia are barrel-shaped, germinate apically and lack fibrosin bodies (Miazzi et al., 2011).

The life cycle of powdery mildew fungi includes asexual and sexual stages, although the asexual cycle appears to be responsible for most of the pathological damage. In the asexual life cycle, three developmental phases can be distinguished after a conidium lands on a susceptible host, as follows: (i) primary appressorium formation and penetration of the cuticle and cell wall, (ii) primary haustorium formation, and (iii) the development of a mat of hyphae (with the formation of secondary appressoria and haustoria) and the differentiation of conidiophores and conidia (Carver et al., 1999; Both et al., 2005b; Romero et al., 2008; Pérez-García et al., 2009; Weßling et al., 2012).

Haustoria, which are specialized fungal structures that develop inside plant epidermal cells, are responsible for the intimate relationship between the pathogen and the host through mediating the uptake of nutrients from the plant (Hahn and Mendgen, 1997; Fotopoulos et al., 2003; Both et al., 2005a; Puthoff et al., 2008; Spanu et al., 2010; Pliego et al., 2013) and the deliverance

* Corresponding author. Fax: +34 952136645.
E-mail address: aperez@uma.es (A. Pérez-García).

http://dx.doi.org/10.1016/j.fgb.2014.08.006
1087-1845/© 2014 Elsevier Inc. All rights reserved.

of virulence effectors (Bindschedler et al., 2009, 2011; Meyer et al., 2009; Grouffaud et al., 2010; Rafiqi et al., 2010; Koeck et al., 2011; Micali et al., 2011; Hacquard et al., 2013). Preliminary studies have provided the first view of the *P. xanthii* haustorium within plant cells, although the fine structure and morphology were unclear. Like those of other powdery mildew species, the *P. xanthii* haustorium resembles a bulb connected to an epiphytic fungal hypha and exhibits the typical tubular elongations called lobules (Cohen et al., 1990; Kuzuya et al., 2006; Fofana et al., 2005). A recent ultrastructural analysis of *G. orontii* haustoria demonstrated additional notable features of powdery mildew haustoria. First, the presence of multivesicular bodies (MVBs) and small vesicles in the haustoria, and second, the occurrence of the progressive encasement of the haustoria by deposits of plant cell-wall polymers produced due to their interaction with the host plant's cells (Micali et al., 2011).

Powdery mildew fungi are a particular group of plant pathogenic fungi with specific host adaptations, including haustoria with different shapes and morphologies. Information about their specific interactions with host plant cells is needed to fully understand the functionality of this structure in fungal development and disease establishment. *P. xanthii* has been identified as the sole causal agent of cucurbit powdery mildew disease in the south of Spain and in many other countries (del Pino et al., 2002; Fernandez-Ortuño et al., 2006). Despite the relevance of haustoria in the life cycle of powdery mildew species, little is known about these structures in *P. xanthii*. In this study, we describe the ultrastructure of *P. xanthii* haustorial complexes using various microscopy techniques. In addition, we report a reliable method for the isolation of *P. xanthii* haustorial complexes from zucchini leaves that allowed the investigation of the occurrence and the pattern of distribution of vesicles in the haustoria. All of our findings were finally integrated into a model of how haustoria establish their intimate interaction with the host cells.

2. Materials and methods

2.1. Fungal isolate, plant material and culture conditions

The *P. xanthii* isolate 2086 was used in this study. The fungal isolate was routinely cultured on zucchini (*Cucurbita pepo* L.) cotyledons cv. Negro Belleza (Semillas Fitó, Barcelona, Spain) that were maintained in Bertrand medium in 8 cm Petri dishes under a 16 h light/8 h dark cycle at 22 °C for one week (Álvarez and Torés, 1997). For the isolation of haustorial complexes, fresh zucchini cotyledons were inoculated by spraying with suspensions of *P. xanthii* conidia and were maintained in Bertrand medium under the conditions described above for 10–14 days to obtain abundant fungal biomass. For the callose deposition assays, we used plants of the melon (*Cucumis melo* L.) cv. Rochet, which are susceptible to *P. xanthii*, and those of cv. PMR-6, which are resistant to *P. xanthii* isolate 2086.

2.2. Isolation of xanthii haustorial complexes

The isolation of haustorial complexes was conducted as previously described by Godfrey et al. (2009), with minor modifications. Approximately 30 zucchini cotyledons that were highly infected with *P. xanthii* (14 days post inoculation) were selected and were dipped in 5% (w/v) cellulose acetate in 100% acetone (Both et al., 2005b). After the evaporation of the acetone, the epiphytic mycelium and conidia were trapped in the solidified cellulose acetate and were removed by stripping the cellulose acetate film from the leaves. The cotyledons were cut into small pieces and homogenized at high speed for 10–15 s in 200–300 ml of ice-cold isolation buffer (0.2 M sucrose, 10 mM MOPS, 1 mM KCl, 1 mM $MgCl_2$, 1 mM $CaCl_2$, pH 7.2) in a kitchen blender. All of the downstream steps were performed at 4 °C. The homogenate was immediately filtered using a coarse stainless steel mesh (80 holes/cm^2), and the filtrate was collected on ice. Material retained by the mesh was further homogenized in 100–200 ml of isolation buffer for 15–20 s and re-filtered. The resulting filtrates were combined and filtered using a fine stainless steel mesh (250 holes/cm^2). The filtrate was centrifuged at 5000 rpm for 10 min and the supernatant was discarded. The pellet was re-suspended in isolation buffer, filtered using a 60 μm nylon filter, and centrifuged at 5000 rpm for 10 min. The resulting pellet was re-suspended in 20 ml of isolation buffer, filtered using an 11 μm nylon filter and centrifuged at 5000 rpm for 10 min. The pellet was re-suspended in 5 ml of isolation buffer and maintained at 4 °C overnight. The slurry that formed at the bottom of the tube contained the haustorial complexes and debris, and the supernatant, which contained mostly chloroplasts, was discarded. The haustorial complexes and debris were re-suspended in 5 ml of isolation buffer and loaded on 5 ml of pure Percoll® (Sigma–Aldrich, USA) in a 15 ml Falcon tube. The sample was centrifuged at 720*g* for 15 min. The haustorial complexes were captured in the fraction comprising 4–6 ml from the bottom and were diluted in 7 ml of isolation buffer and centrifuged at 5000 rpm for 10 min. The pellet was re-suspended in 1 ml of isolation buffer. After staining using WGA-Alexa Fluor 488® conjugate (Invitrogen, USA), confocal laser scanning microscopy was used to assess the presence and purity of the haustorial complexes in the final suspension.

2.3. Confocal laser scanning microscopy (CLSM)

We examined the haustoria *in planta* and isolated by CLSM. For *in planta* examination, infected leaf discs were cleared using 96% ethanol at 95 °C and then washed for 20 min in phosphate-buffered saline. The fungal cell walls were labeled by incubating the specimens at 4 °C overnight in a solution of 0.05 mg/ml WGA-Alexa Fluor 488® conjugate in PBS. For examination of the isolated haustoria, the haustorial complexes were labeled using 0.025 mg of WGA-Alexa Fluor 488® conjugate per ml in PBS. The 3D projected images were obtained using haustorial complexes labeled with 0.05 mg of WGA-Alexa Fluor 488® conjugate per ml in PBS. To label the haustorial nuclei, the isolated haustorial complexes were centrifuged at 5000 rpm for 10 min and were re-suspended in 2 μg/ml DAPI (4,6-diamidino-2-phenylindole-dihydrochloride) (Sigma–Aldrich) in 0.1% Tween 20 in PBS for 30 min. The fungal membranes were stained using a 0.02 mg/ml solution of SynaptoRed™ C2 (also known as FM4-64) for 10 or 30–40 min (Sigma–Aldrich). To visualize the callose deposits, disks of *P. xanthii*-infected leaves were cleared in an ethanol dilution series of 50–100% and were stained by immersion for 12 h in a solution of 0.01% aniline blue in K_2HPO_4 (7 mM, pH 8.9). The disks were then mounted in 0.01% calcofluor (Sigma–Aldrich) on glass slides to stain fungal colonies. The samples were observed using a Leica SP5 II confocal microscope (Leica Microsystems GmbH, Wetzlar, Germany). All of the images were obtained using a 63x oil-immersion objective and were processed using Leica LAS AF software (LCS Lite, Leica Microsystems) and Adobe Photoshop CS5 software.

2.4. Image analysis

Image rendering of haustorial complexes and quantifications of fluorescence intensity of callose and vesicles and the size of haustoria were done using the free Java image processing software ImageJ. The 3D projected images of haustorial complexes were obtained using 50–100 confocal image stacks or z-stacks (0.13–0.14 μm interval). To analyze the relationship between callose fluorescence

and haustorial area, micrographs obtained from aniline blue staining were used. To quantify the fluorescence associated to vesicles from haustorial lobes and bodies, micrographs obtained from FM4-64 labeling were used.

2.5. Transmission electron microscopy (TEM)

The samples were fixed overnight at 4 °C using 3% glutaraldehyde in 0.1 M cacodylate buffer, pH 7.2, containing 0.1 M sucrose. After washing in buffer, the samples were post-fixed for 2 h at room temperature using 1% osmium tetroxide in the same buffer. The samples were dehydrated in an acetone series (30%, 50%, 70%, 80%, 90%, and 100% acetone). The acetone was replaced with a 1:1 mixture of Araldite 502 (EMS, UK) resin and 100% acetone. After 2 h of incubation at room temperature, the samples were incubated for 2–4 h at room temperature in 100% resin. Finally, the samples were placed in molds containing 100% resin and polymerized at 60 °C for 48 h. To evaluate the quality of inclusions and select the areas containing *P. xanthii* structures, the polymerized blocks were trimmed and semithin 1 µm tissue sections were mounted on glass slides, stained with 0.05% toluidine blue and examined under a light microscope. For TEM observation, the trimmed blocks were sectioned at 70–90 nm using an ultramicrotome Om U3 (C. Reichert, Austria), mounted on copper grids, stained using a 1% uranyl acetate solution for 45 min and examined using a Philips CM-200 transmission electron microscope.

3. Results

3.1. Structure of P. xanthii haustorial complexes within plant cells

Haustoria, the organs directly responsible for pathogen-host interaction in obligate biotrophic fungi, have been poorly investigated in the cucurbit powdery mildew fungus *P. xanthii*. A better understanding of haustorial functionality undeniably implies a better knowledge of their structure. Thus, we first decided to study the assembly of haustoria during the intimate interaction of *P. xanthii* with susceptible host plants. To do so, we assessed their presence and appearance within the host plant using the cell wall-specific stain WGA-Alexa Fluor 488® conjugate and confocal laser scanning microscopy (CLSM) (Fig. 1). Using DIC microscopy, the haustoria appeared as dark globular structures perfectly delimited within the less contrasted plant cells (Fig. 1A). These globular structures were then labeled with WGA-Alexa Fluor 488® conjugate that binds specifically to residues of chitin (N-acetyl-D-glucosamine) and subjected to CLSM analysis, as previously performed to visualize the haustoria of other fungal species (Miklis et al., 2007; Bindschedler et al., 2009). We could roughly distinguish a core, presumably the haustorial body and closely associated tubular structures that we identified as the haustorial lobes (Fig. 1B).

To determine the ultrastructural anatomy of the haustoria, we next conducted a transmission electron microscopy (TEM) analysis. Semithin sections of densely infected cotyledons embedded in resin were evaluated for their quality and the presence of fungal haustoria using toluidine-blue staining and bright-field light microscopy (Fig. 2). In most of the sections, the haustorial complexes were observed within the plant epidermal cells, adjacent to fungal hyphae on the plant surface (Fig. 2A). A hypha and a haustorium were connected by a highly stained filamentous structure, the haustorial neck, which appeared embedded within a cylindrical papilla, the formation of which is a typical plant response to pathogen invasion and which is highly reactive with toluidine-blue stain due to being composed of callose and lignin polymers, among other compounds (Meyer et al., 2009; Wen et al., 2011). The innermost sections of these haustorial complexes revealed a haustorial body surrounded by irregular lobe-like structures (Fig. 2B). TEM analysis of these samples allowed us to distinguish two morphologically different developmental stages of the haustorium: (i) an immature haustorium with a small haustorial body and lacking any recognizable subcellular features (Fig. 3A), and (ii) a mature haustorium that is larger and is highly structured (Fig. 3B–D). The central zone of a mature haustorial body was mainly occupied by large vacuoles, with a few electron-dense vesicles. Several lobes surrounded the haustorial body, and some of these lobes shared the cytoplasm and cell wall of the haustorial body (Fig. 3B, arrowhead). The haustorial body and lobes were embedded within an extrahaustorial matrix and separated from the plant cytoplasm by the outer electron-dense extrahaustorial membrane (Fig. 3A–B). A higher magnification image shows the irregular topology of the extrahaustorial membrane and the presence of some short projections (Fig. 3C, arrowhead), both features that are typically associated with the haustoria of other powdery mildew species (Gil and Gay, 1977; Voegele and Mendgen, 2003).

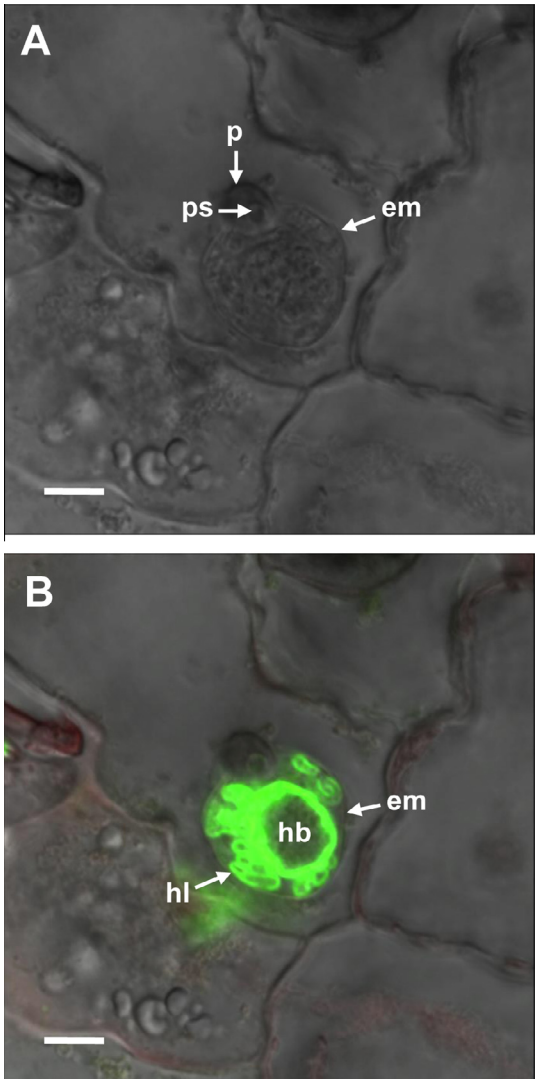

Fig. 1. Structure of an intact haustorium of *P. xanthii* that developed inside an epidermal cell of a zucchini cotyledon. (A) DIC micrograph showing a haustorial complex surrounded by the extrahaustorial membrane (em) and the fungal penetration site (ps) in the middle of a plant papilla (p). (B) Confocal laser scanning micrograph of an WGA-Alexa Fluor 488® conjugate-labeled haustorium showing the haustorial body (hb), the haustorial lobes (hl) and the extrahaustorial membrane (em). Bars: 5 µm.

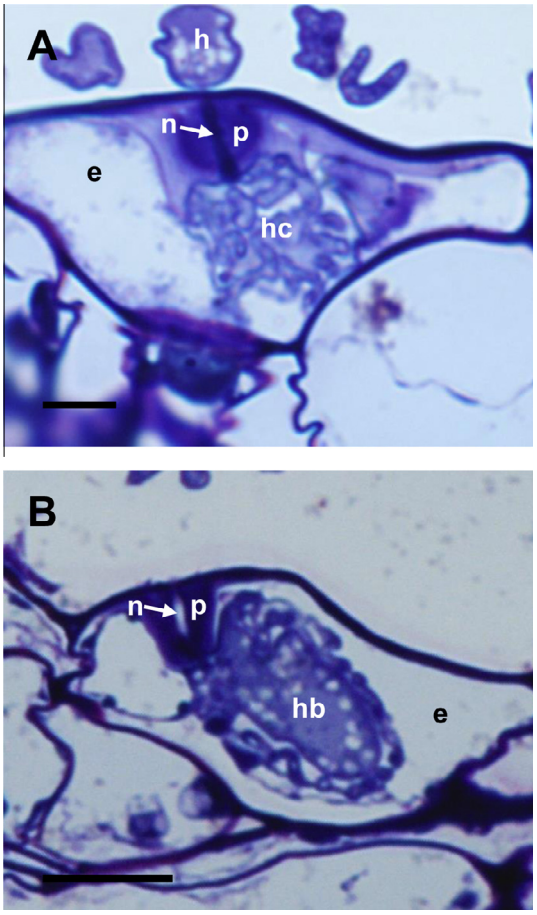

Fig. 2. Visualization of resin-embedded melon leaves infected with *P. xanthii*. Thin sections were stained with 0.05% toluidine blue and were analyzed using bright-field microscopy. (A) An outermost section showing a haustorial complex (hc) inside of a epidermal plant cell (e) that is attached to a floating fungal hypha (h) by the neck, which crosses the more densely stained plant papilla (p). (B) An innermost section of a haustorial complex showing a haustorial body (hb). Bars: 5 μm in A and 10 μm in B. (For interpretation of the references to colour in this figure legend, the reader is referred to the web version of this article.)

The outermost sections of the haustoria revealed a completely different picture, with accumulations of electron-dense plaques of putative plant compounds that covered most of the surface of the haustoria (Fig. 3D).

3.2. Callose deposition and haustorial maturity

In response to fungal infection, plants assemble an encasement, a local defense barrier dedicated to restraining further fungal growth (An et al., 2006; Meyer et al., 2009; Wang et al., 2009). Thus, we asked if the plaques observed on the haustoria in the ultrastructural studies (Fig. 3D) could be part of the plant encasement. For this reason, we decided to analyze the callose deposits because it is the main component of encasement. To study this issue, *P. xanthii*-infected leaves were stained with aniline blue, a stain widely used to detect callose deposits in plants, and examined using CLSM microscopy (Fig. 4). As previously observed using DIC microscopy, the haustoria were recognized as bordered darker areas within the plant epidermal cells (Fig. 4A). The callose deposits nearly covered the *P. xanthii* haustoria (Fig. 4B and C) in a pattern that resembled the distribution of plaques around the haustorial complexes that was observed in the TEM studies (Fig. 3D). Interestingly, during the interaction with a resistant melon cultivar, the fluorescent signal associated with callose extended below the fungal penetration points and merged to completely cover the surface of the haustoria (Fig. 4D). These findings suggested the presence of callose in the plaques and indicated a progression of the spatial pattern of callose deposition dependent on the developmental stage of the *P. xanthii* colonies (Fig. 5). Indeed, we found that in the center of colonies, which contained mainly mature haustoria, the plaques of callose deposits extended below the fungal penetration points and wrapped completely the haustorial complexes (Fig. 5C and E). However, in the periphery of the colonies, which were enriched in young and immature haustoria, the callose deposition was limited to the fungal penetration points, presumably as result of papilla formation (Fig. 5D and F). To verify these results, the intensity of callose fluorescence and haustorial area were measured and correlated with each other (Fig. S1) and differentiated two defined groups of haustoria depending on size and fluorescence intensity: young and immature haustoria and mature haustoria. These results showed a positive correlation between haustorial maturity and callose deposition.

3.3. Haustorial lobes and haustorial maturity

One of the most remarkable changes in the maturation of haustoria is the formation of the haustorial lobes, tubular projections that emerge from the haustorial body (Figs. 1A and 3) (Manners and Gay, 1977; Micali et al., 2011). To investigate the relevance of this morphological feature in the functionality of haustoria, we examined haustoria after isolation as described in Section 2 (see Fig. 2S). The integrity of the purified haustoria was evaluated by CLSM and double staining with DAPI and the Alexa Fluor probe (Fig. 6). The appearance of the purified haustoria was reminiscent of the haustoria that developed within plant cells (Fig. 1A); the haustorial body was closely associated with the outermost haustorial lobes, both of which were reactive with WGA-Alexa Fluor (in green), and the nucleus was stained with DAPI (in blue) (Fig. 6B and C). In addition to these findings, the neck of a haustorium and the underlying septum could be discriminated in some haustoria (Fig. 6B–C and E–F, respectively). Mature haustoria ($n = 20$) measured 20.95 μm (±1.29) × 16.03 μm (±1.56), whereas the immature haustoria were 15.3 μm (±0.46) × 11.3 μm (±0.37); the haustorial body was 10.98 μm (±0.88) × 6.86 μm (±0.81); and the haustorial septum was 1.43 μm (±0.14) in length.

The formation, appearance and distribution of lobes in purified haustoria also appeared correlated with maturation (Fig. 7). Young haustoria exhibited only a few lobes, which emerged mainly from the region near the haustorial neck at some distance from the haustorial body (Fig. 7A). The number of lobes increased considerably in mature haustoria and decorated nearly the entire surface (Fig. 7B and C, Video S1). The size of the lobes also changed over time. Initially, the lobes arose from the haustorial cell wall (Fig. 7D and E, arrowhead), and appeared tube-like, and widened with age (Fig. 7B and C, Video S1). Also note the presence of orifices in the haustorial body near its neck and at the opposite end at the location where lobes joined with the haustorial body. In the immature haustoria, these orifices were an average of 0.66 μm in diameter (Fig. 7A, arrows), whereas in the mature haustoria, the orifices were up to 2 μm in diameter (Fig. 7B, arrows). Thus, we considered these orifices as an additional morphological feature of the lobes that reflect the maturation of haustoria.

3.4. Haustorial lobes mediate vesicle trafficking during the interaction of *P. xanthii* with host cells

A persistent biotrophic interaction is maintained when the damage caused to the host cells is in balance with the intensity of the plant-defense response triggered by its parasite. The formation of vesicles appears to be an efficient way to control the deliverance

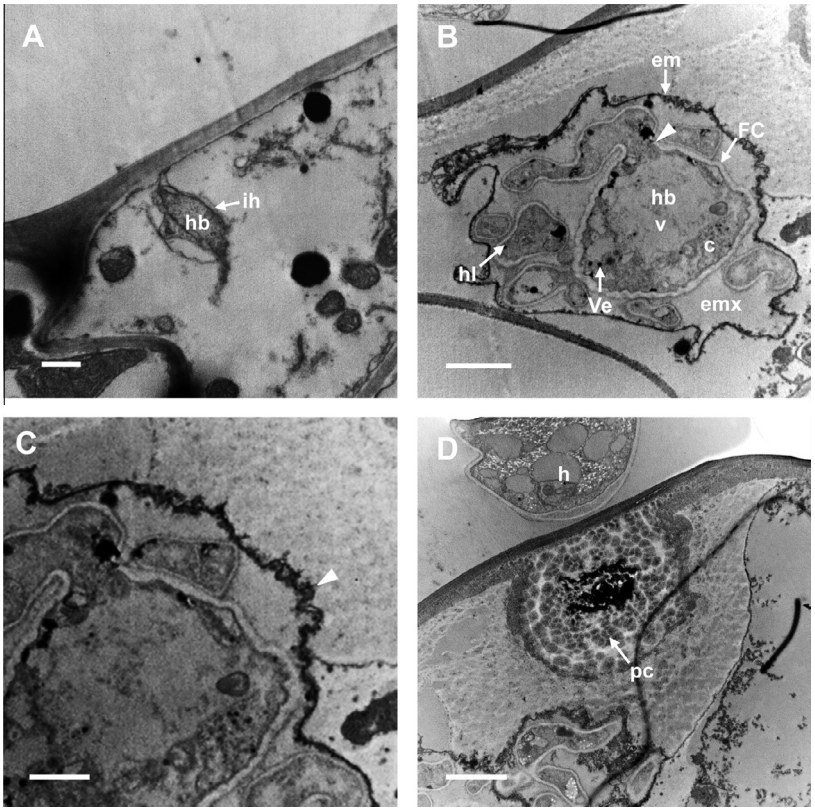

Fig. 3. Development of *P. xanthii* haustoria within melon-plant cells. Ultrathin sections of resin-embedded *P. xanthii*-infected melon leaves containing haustorial complexes were stained with uranyl acetate and were visualized using TEM. (A) A featureless immature haustorium (ih) with a naked, small haustorial body (hb). (B) Transverse section of a mature haustorium: The haustorial body (hb) is occupied by a large vacuole (v), a small amount of cytoplasm (c) and several vesicles (Ve). Haustorial lobes emerge from the haustorial body (arrowhead), sharing the cell wall (FC) and cytoplasm. The haustorium is separated from the extrahaustorial membrane (em) by the extrahaustorial matrix (emx). (C) A higher-magnification image of the extrahaustorial membrane from image B showing its irregular structure and the presence of short projections (arrowhead). (D) A haustorial complex externally covered by plaques of putative plant compounds (pc). h, hypha. Bars: 0.5 μm in A; 5 μm in B; 2 μm in C and 2.5 μm in D.

of pathogenic effectors in these biotrophic interactions and maintain this equilibrium (Rodrigues et al., 2008; Micali et al., 2011). Thus, we speculated that the haustoria would contain most of such transport structures. To study this issue, we performed CLSM analysis of isolated haustoria doubly stained with WGA-Alexa Fluor probe for cell-wall labeling (green) and FM4-64 for membrane staining (red) (Fig. 8). Short exposure to the FM4-64 dye specifically stained (red) the plasma membrane of the haustoria, the extrahaustorial membrane (EHM) wrapping an entire haustorium and other membranous structures, such as several types of smaller vesicles, but not the nuclei or mitochondria (Fig. 8B and C). The haustorial membrane covered not only the body but also the closely associated lobes, as occurs with the cell wall and a region of the haustorial neck above the septum (arrowhead) that did not exhibit a cell wall (arrow) (Fig. 8A–C). In addition, the haustorial complexes contained abundant large- (arrow) and medium-sized vesicles (arrowheads) (Fig. 8D–F). We also observed nuclei (Lewis et al., 2009) that were stained only with exposure times of 30–40 min (Fig. 8H). Surprisingly, red fluorescence signal showed a differential pattern of distribution between haustorial body and haustorial lobes. In mature haustoria, the haustorial body cytoplasm was mostly free of signal, with some medium- and large-sized vesicles located in the periphery (Fig. S3A). By contrast, the haustorial lobes were occupied by a cloud of small FM4-64 stained vesicles, as well as abundant medium- and large-sized vesicles (Fig. 8F, Fig. S3B, Videos S2 and S3). The examination of a gallery of individual confocal optical sections obtained from a single isolated haustorium (Fig. S4) and the quantification of the fluorescence intensity associated to the vesicles in the haustorial lobes and the haustorial body (Fig. S5) supported of this observation.

Not surprisingly, the immature haustoria, which had lobes of variable density, did not exhibit medium- or large-sized vesicles but rather small vesicles within a lobe that was budding from the haustorial body (Fig. 8G, arrowhead). Finally, higher-magnification images of the extrahaustorial matrix allowed us to distinguish some small vesicles near the EHM and the lobes that we tentatively propose to be exosomes (Fig. 8I, arrowhead) based on the similarity of their sizes and localization to those reported in previous studies (Schorey and Bhatnagar, 2008; Micali et al., 2011; Théry, 2011).

4. Discussion

P. xanthii is a very significant pathogen of cucurbits. The intense research done on the plant response to *P. xanthii* contrasts with the scarce information available on the pathogenic process of this fungus and its development in compatible or incompatible hosts (Fofana et al., 2005; Sedlářová et al., 2009). One of the most fascinating organs involved in this biotrophic interaction is the haustorium; thus, we first asked how similar the structure of this organ in *P. xanthii* would be to those of the diverse group of powdery mildew fungi. In our *in vivo* study using CLSM and an Alexa Fluor conjugate probe, non-manipulated haustoria were visualized and at least three of their structural parts were distinguished: the body, lobes and neck (Fig. 1). The preliminary observations of the haustoria resembled that previously reported in pioneer TEM microscopy studies of *P. xanthii* and in the powdery mildew species *Erysiphe pisi* (Gil and Gay, 1977), *Blumeria graminis* f. sp. *hordei* (Panstruga, 2003) and *G. orontii* (Micali et al., 2011). However,

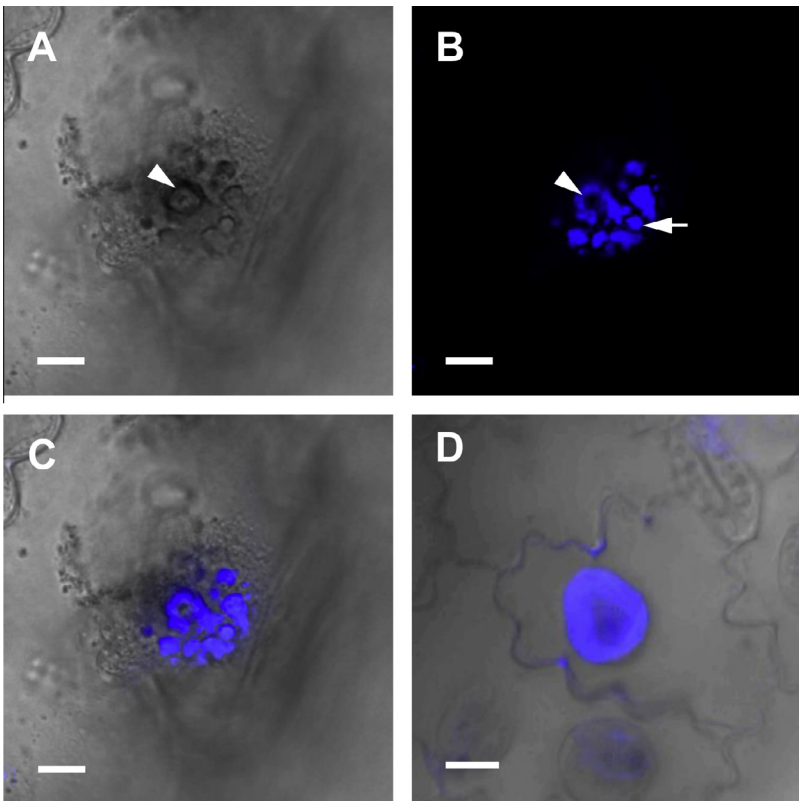

Fig. 4. Development of callose deposits in melon plants infected with *P. xanthii*. Confocal laser scanning micrographs showing aniline blue fluorescence within a susceptible plant (B-C) and a resistant plant (D). (A) DIC micrograph showing a haustorial complex under the point of fungal penetration (arrowhead). (B) CLSM micrograph showing the haustorial complex surrounded by plaques of callose deposits (arrow) near the penetration point (arrowhead). (C) Overlay of DIC and CLSM images showing callose deposits inside the plant cell. (D) Overlay of DIC and CLSM images of a haustorial complex developed in a resistant melon plant of cv. PMR-6. In this case, the haustorial complex is completely surrounded by callose. Bars: 5 μm in A-C and 10 μm in D. (For interpretation of the references to colour in this figure legend, the reader is referred to the web version of this article.)

we have determined that the haustoria of *P. xanthii* exhibit some unique morphological features. First, the size of the *P. xanthii* haustorium (20.95 μm × 16.03 μm) is greater than that of *G. orontii* (16.2 μm × 10 μm) (Micali et al., 2011). Secondly, in *P. xanthii*, the haustorial lobes emerge from the neck region as well as from the opposite end of haustorial complexes and almost completely cover the haustorial body (Fig. 7). Not surprisingly, this distribution of lobes has also been observed in other powdery mildew species, such as *E. pisi* (Gil and Gay, 1977) and *G. orontii* (Koh et al., 2005; Micali et al., 2011), but differ from that of *B. graminis* f. sp. *hordei*, in which the lobes grow as finger-like projections at the poles (Koh et al., 2005; Godfrey et al., 2009). These morphological differences in the haustoria change the amount of haustorial surface area in contact with the host cells, which may result from physical limitations imposed by the host cells. Indeed, the hosts of *B. graminis* are monocotyledons, whereas the hosts of the other powdery mildew species mentioned are dicotyledons, which have morphologically different epidermal cells. Thus, we hypothesize that during the evolutionary process, each powdery mildew species has adapted the architecture of their haustoria to their host but conserved its functionality.

The variations in structure that were observed using CLSM were confirmed in the TEM studies, which also allowed us to investigate the ultrastructure of the haustorium in detail. Transverse ultrathin sections of *P. xanthii* haustoria revealed the presence of an extrahaustorial membrane highly irregular in outline (Fig. 3C) that was similar to that reported in *B. graminis*, *E. pisi* and *G. orontii* (Gil and Gay, 1977; Micali et al., 2011). We also observed that the haustorial body cytoplasm is almost completely occupied by a large vacuole that is surrounded by several vesicles (Fig. 3B). This anatomy of the haustoria led us to consider a reasonable division of functions: the central haustorial body is mainly dedicated to the synthesis of proteins and of effectors, which must to be secreted, and the metabolism of nutrients obtained from the plant cells; whereas the haustorial lobes are responsible primarily for the exchange of factors and effectors with plant cells, nutrient uptake and nutrient delivery to the haustorial body.

The outermost sections of the haustoria revealed an interesting finding: plaques deposited on the haustoria (Fig. 3D), quite possibly derived from the plant host. For this reason, we examined callose deposits using aniline blue staining. Callose and other deposited polymers constitute a plant papilla, one of the first plant structures formed in response to a pathogen attack, which restrains further pathogen progress (An et al., 2006; Meyer et al., 2009; Wang et al., 2009; Wen et al., 2011; Ellinger et al., 2013; Naumann et al., 2013; Eggert et al., 2014). However, in the *P. xanthii*-compatible melon plant interactions, this response is insufficient (Romero et al., 2008). In fact, intact haustorial necks crossed the plant papilla that had formed below each penetration point, allowing the unimpeded growth of fungal hyphae over the plant surface (Fig. 2). Interestingly, callose deposition progressed in parallel with haustorial development (Fig. S3), starting near the haustorial neck to completely embed the haustorial complexes (Fig. 4). Why does that deposition not stop fungal growth? We have previously demonstrated that susceptible and resistant melon cultivars deploy the same mechanisms to prevent *P. xanthii* infection (Rivera et al., 2002; Romero et al., 2008). However, the level of accumulation of cell-wall deposits, such as callose, was

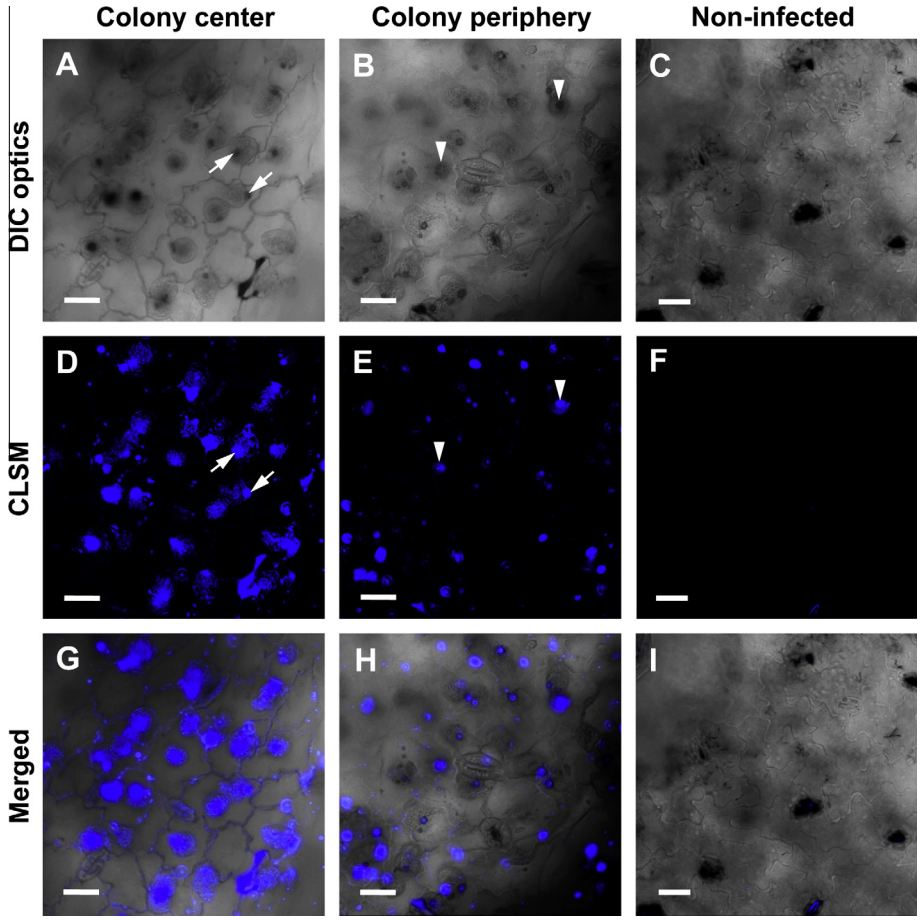

Fig. 5. The pattern of callose deposition varies depending on the developmental stage of the haustoria of *P. xanthii*. Leaf disks of susceptible melon cultivars bearing colonies of *P. xanthii* were stained with aniline blue and were analyzed using confocal laser scanning microscopy. (A-B) DIC micrographs of haustorial complexes formed below the penetration point of the plant epidermal cells (arrowheads and arrows). (C) Absence of haustoria into epidermal cells of non-infected leaf. (D–F) Confocal laser scanning micrographs of aniline blue-stained melon leaves showing, the accumulation of the fluorescence signal within a small papilla in response to peg penetration (arrowheads) at the periphery of a colony dominated by young haustoria, whereas, D, plaques of callose deposits surround the haustorial complexes (arrows) in the middle of a colony dominated by mature haustoria. (F) Note the absence of fluorescence signal in non-infected leaves. (E–I) Overlaid images of (A-D), (B-E) and (C-F). Bars: 5 μm in A-C and 10 μm in D-F. (For interpretation of the references to colour in this figure legend, the reader is referred to the web version of this article.)

comparatively low in the susceptible melon plants compared to the resistant counterparts (Fig. 4), which generated a delay in the spatio-temporal pattern of its deposition and, in consequence, inefficacy in restraining further fungal progress (Romero et al., 2008). Consistent with this data, in the periphery of *P. xanthii* colonies, callose was deposited under all of the penetration points, corresponding to the sites of the papillae; however, in the middle of the colony, which is dominated by mature haustoria, these sites were surrounded by plaques of callose that failed to enclose the entire haustorial complexes, hypothetically letting *P. xanthii* proliferate (Figs. 4 and 5). Although, we cannot determine how the pathogen modulates callose deposition, we might hypothesize a mechanism similar to what is known in other powdery mildew-host interactions. For example, in the interaction of *B. graminis* f. sp. *hordei* and barley, the fungus triggers the expression of the plant defense protein MLO (Opalski et al., 2005; Miklis et al., 2007; Schultheiss et al., 2008). This defense protein induces the reorganization of actin filaments, which diffusely surround the haustorial complexes, directing the accumulation of callose (Olesen et al., 2003; Lipka and Panstruga, 2005; Eichman and Hückelhoven, 2008). The identification in melon of *CmMlo1* (Cheng et al., 2012), orthologous to barley *Mlo*, suggests a similar mechanism for callose deposition around *P. xanthii* haustoria, although this idea needs to be investigated further.

Haustorial lobes are projections that are present in the haustoria of different powdery mildew species (Koh et al., 2005; Eichman and Hückelhoven, 2008) and that communicate with the haustorial body. We have observed that in *P. xanthii*, the lobes emerged from both "ends" of the haustorium (Fig. 6E and Fig 7A and B), similar to those of *G. orontii* (Micali et al., 2011) and *B. graminis* f. sp. *hordei* (Godfrey et al., 2009). Our observations of haustoria of different ages led us to propose the presence of haustorial lobes as an indication of the maturity of the haustorium; small lobes indicate young haustorial complexes and large lobes indicate mature complexes. In addition, our study has allowed us to deepen our understanding of haustorial functionality. Two findings indicated the involvement of haustorial lobes in the communication of *P. xanthii* with host cells: (i) they cover nearly the entire surface of the haustorial body (Fig. 7C and Video S1), which increases the surface area in contact with the host cells and facilitates the exchange of material (Eichman and Hückelhoven, 2008), and (ii) their cell wall is thinner than the haustorial body (Fig. 3B arrowhead), which presumably would favor vesicle secretion and transit (Rodrigues et al., 2008). Evidence supporting this hypothesis has been observed in yeast cells, in which highly active vesicular transit occurs near the thinner growing areas of their cell walls (Rodrigues et al., 2008). The vesicular pathway has been extensively studied in yeasts and numerous filamentous fungi

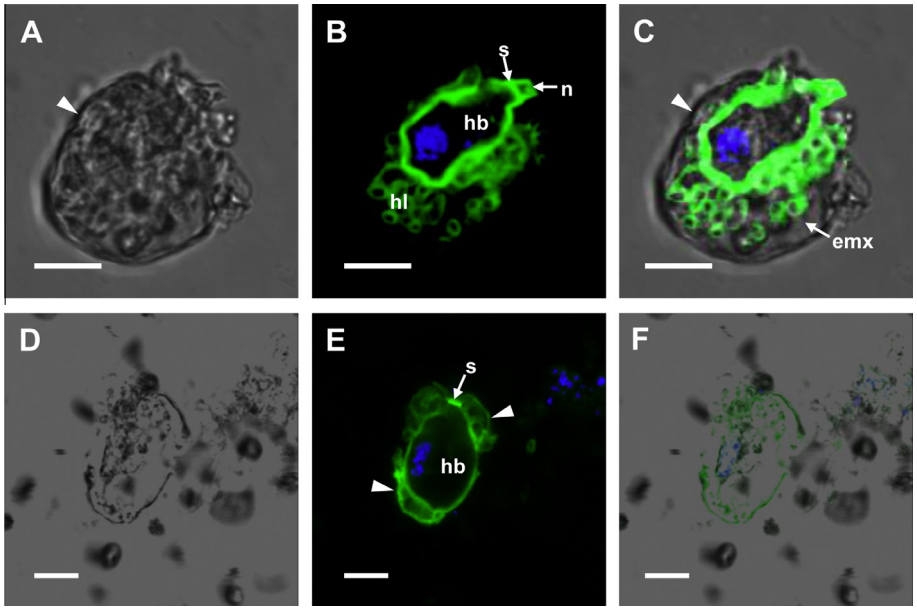

Fig. 6. Isolated haustoria of *P. xanthii* preserved their structural integrity. A and D. DIC micrographs showing the morphologically distinct mature or young haustoria. B and E. Confocal laser scanning micrograph and double labeling with DAPI and WGA-Alexa Fluor 488® conjugate staining. B. A mature haustorium with the nucleus (in blue) contained within a haustorial body (hb), with peripheral haustorial lobes (hl) and a septum (s) in a polar haustorial neck (n). E. A young haustorium with the nucleus (in blue) contained within a naked haustorial body, with a septum (s) and haustorial lobes emerging from the neck region as well as from the opposite end of the haustorial body (arrowheads). C and F. Overlay of the images in panels A and B and D and E, respectively. Bars: 5 μm. (For interpretation of the references to colour in this figure legend, the reader is referred to the web version of this article.)

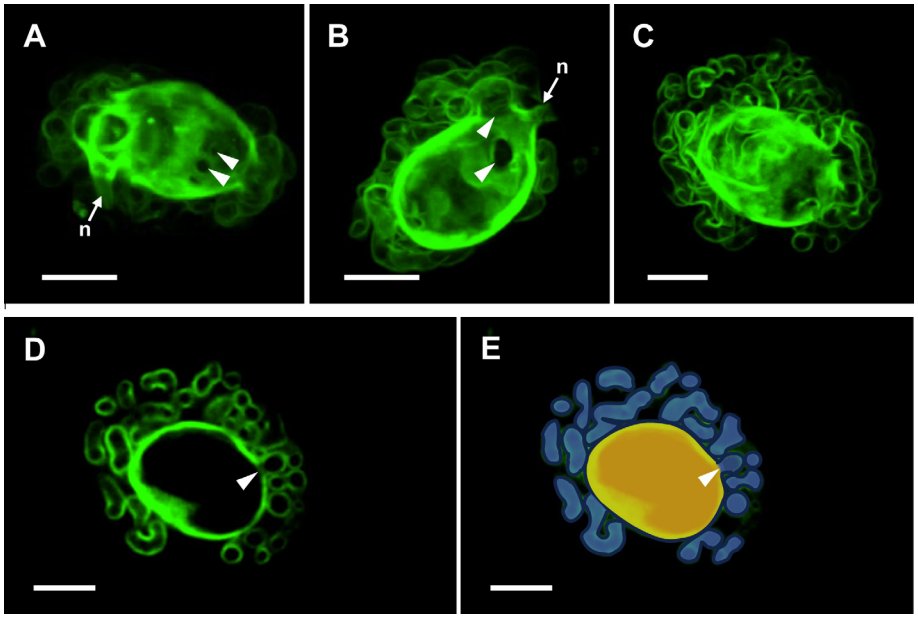

Fig. 7. The number and distribution of *P. xanthii* haustorial lobes increased in parallel with haustorial development. Haustoria at different developmental stages were labeled with the WGA-Alexa Fluor 488® conjugate probe and analyzed using CLSM microscopy. (A and B) Immature haustorial complexes have lobes emerging from the neck the region (n) as well as from the opposite end of the haustorial body (arrows). (C) Mature haustorial complexes are completely surrounded by haustorial lobes. (D) Detail of a section of a haustorial complex with some lobes emerging from the cell wall (arrowhead). (E) Image of a false-colored mature haustorium with the haustorial body (yellow) completely surrounded by the tubular lobes (blue) and a lobe arising from the cell wall (arrowhead). Bars: 5 μm. (For interpretation of the references to colour in this figure legend, the reader is referred to the web version of this article.)

(Fischer-Parton et al., 2000). These studies revealed that vesicular trafficking in these organisms is highly organized and involves the activities of various vesicles of different sizes. In contrast, little is known about vesicular trafficking in powdery mildew species, and more precisely, about haustorium functionality.

We have adapted a reliable method to purify intact *P. xanthii* haustoria that can be used to study the presence of vesicles, their variety and their functionality during the interaction of haustoria with host cells. To visualize vesicles in the lobes, we used one of the FM dyes, a family of membrane-selective fluorescent dyes commonly used to label and monitor synaptic vesicles, secretory granules and other endocytic/exocytic structures in a variety of organisms (Fischer-Parton et al., 2000). As expected from the proposed role of lobes in the intimate communication of haustoria

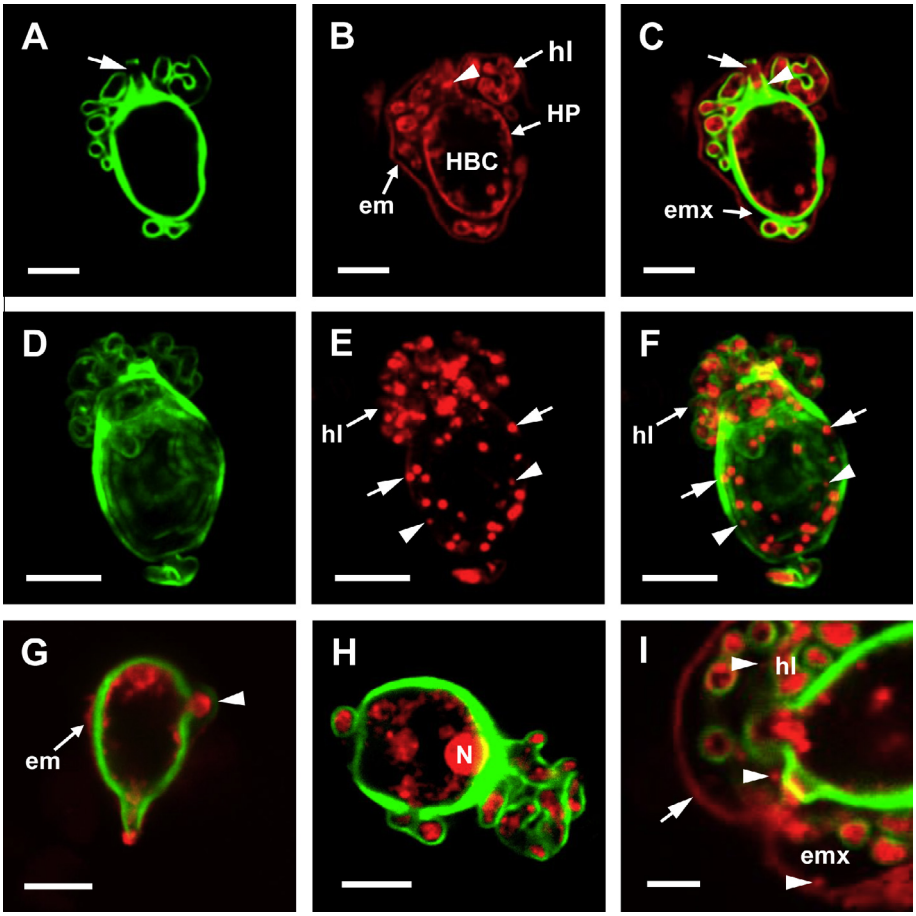

Fig. 8. Pattern of distribution of putative vesicles in purified *P. xanthii* haustoria. Isolated haustorial complexes were labeled with WGA-Alexa Fluor 488® conjugate (green; A, D) and FM4-64 (red; B, E) and were analyzed using confocal laser scanning microscopy. (A) A representative isolated haustorium showing the haustorial neck with an area devoid of a cell wall (arrow). (B) Specific staining of the extrahaustorial membrane (em), the haustorial plasma membrane (HP), the haustorial lobes (hl) and the septum (arrowhead) with FM4-64. The cytoplasm (HBC) remains unlabeled. (C) Overlay of images A and B showing that the two fluorescence signals coincided in the septum (yellow) but not in the extrahaustorial matrix (emx), which displayed red fluorescence. (D-F) After 5 min of exposure to FM4-64, the haustorial complexes showed more intense fluorescence in the haustorial lobes than in the haustorial bodies. Numerous large- (arrows) and medium-sized entities (arrowhead) that reacted with FM4-64 are visible. (G) The immature haustoria exhibited intensive fluorescence signals in the growing haustorial lobes (arrowhead). In addition, the external membrane appeared to be closely attached to the haustorial cell wall, with no visible extracellular matrix. (H) After 30 min of exposure to FM4-64, the HBC displayed a slightly stained nucleus (N). (I) Putative exosomes (arrowheads) reactive with FM4-64 were concentrated in the extracellular matrix near the haustorial lobes (hl) and the extracellular matrix (arrow). C, F and G-I. Overlay of images of the fluorescence signal from the two respective dyes. Bars: 5 μm in A-G, 4 μm in H and 2.5 μm in I. (For interpretation of the references to colour in this figure legend, the reader is referred to the web version of this article.)

with the host cells, the fluorescent signal associated with membranous entities in the haustorial lobes was higher than that in the haustorial bodies (Figs. S3–S5, Videos S2 and S3). The cytoplasm of the lobes was completely occupied by a cloud of these vesicles, which appeared to be normal for the hyphae of other filamentous fungi (Fischer-Parton et al., 2000; Bolte et al., 2004). The cited studies also showed that the apical region of the growing hyphae of filamentous fungi accumulated an intense fluorescent signal due to the high levels of secretory vesicles called Spitzenkörper that merge with the plasma membrane (Fischer-Parton et al., 2000). Interestingly, in our study, the primary lobes that emerged from young haustorial bodies also showed foci of intense fluorescence, which could be interpreted as the result of the high level of these vesicles (Fig. 8G).

A recent study of the ultrastructure of *G. orontii* haustoria showed the presence of lipid bilayer-containing vesicles of different sizes called multivesicular bodies (MVBs) (Micali et al., 2011). MVBs are generated by the inward budding of the delimiting membrane of endosomes, followed by the release of vesicles into the endosomal lumens (Rodrigues et al., 2008; Théry, 2011). In our study, we also observed the presence of medium- and large-sized vesicles inside of the haustorial cytoplasm of *P. xanthii* (Fig. 8) whose sizes were consistent with the MVBs described previously in *G. orontii* (Micali et al., 2011). In addition and as previously observed for other vesicles, the density of medium- and large-sized vesicles were higher in the cytoplasm of haustorial lobes than in that of the haustorial body (Fig. 8F, Figs. S3–S5, Videos S2 and S3). Previous reports proposed that the MVBs are the vehicles for the transport of small vesicles to vacuoles or, more interestingly, for the release of small vesicles called exosomes (30–100 nm diameter) to the extracellular environment through fusion with the plasma membrane (Valadi et al., 2007; Rodrigues et al., 2008; Schorey and Bhatnagar, 2008; Théry, 2011). We observed the accumulation of small vesicles in the EHMx, always near the EHM and the haustorial lobes (Fig. 8I arrowheads), and based on previous reports, we propose that these small vesicles are putative exosomes that were secreted into the EHMx via MVB fusion with the haustorial membrane. In powdery mildew haustoria, exosomes can play an important role in haustorial establishment and may represent an efficient mechanism for the delivery of fungal

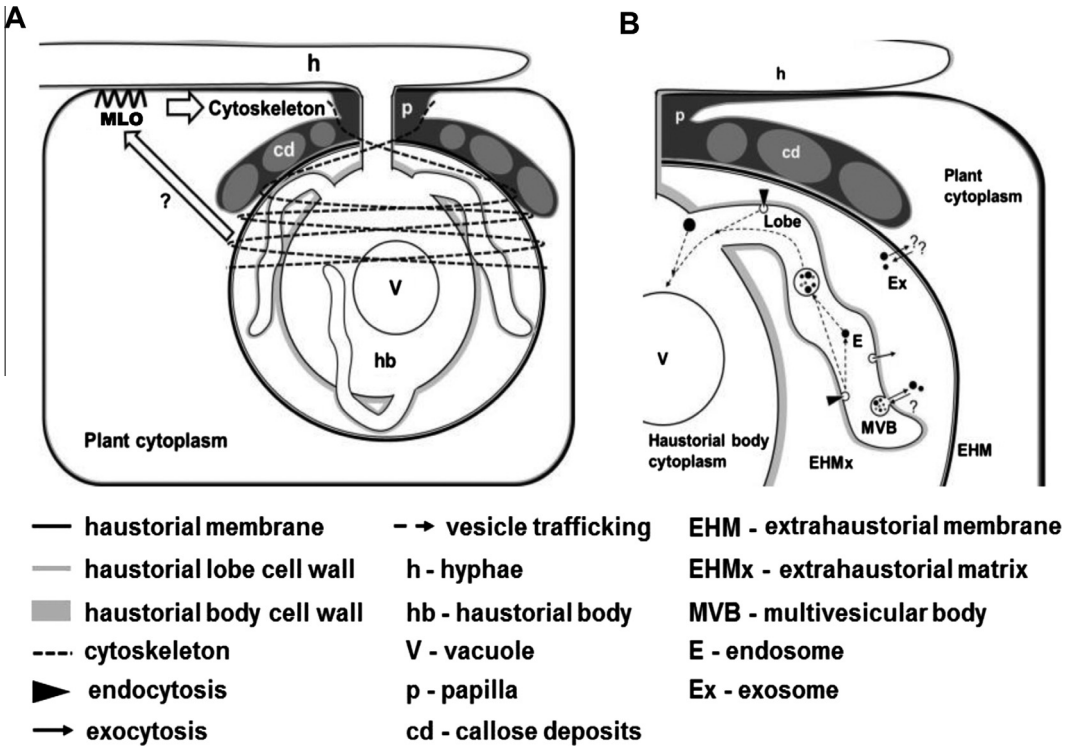

Fig. 9. Schematic representations of the interaction of *P. xanthii* haustoria and plant host cells. (A) Model of the distribution of callose deposition around the haustorial complex. (B) Model of vesicular trafficking in *P. xanthii* haustorial complexes. See text for details.

effectors (Rodrigues et al., 2008), proteins, microRNAs and mRNAs (Valadi et al., 2007). The microRNAs transferred through exosomes can confer new functions on the receptor cells (Schorey and Bhatnagar, 2008), or in these cases, the RNAs transferred could modulate the plant's defense response.

The origin of the extracellular membrane that covers the entire haustorial complex remains controversial. The two following hypothetical pathways exist: *de novo* synthesis of its components or the modification of the plasma membrane of the plant cell (Mackie et al., 1993; Koh et al., 2005; Wang et al., 2009; Lu et al., 2012) by the successive fusion of fungal vesicles. The second hypothesis appears to be the most plausible, at least in powdery mildew fungi. First, we have shown the selective accumulation of vesicles in the EHM near the extrahaustorial membrane. Secondly, the irregular structure of the extracellular membrane of *P. xanthii* haustoria (Fig. 3C), which was also observed in other powdery mildew fungi (Gil and Gay, 1977; Voegele and Mendgen, 2003; Micali et al., 2011), is proposed to be the consequence of a large number of secretory vesicles fusing with the plant plasma membrane. Torralba and Heath (2002) proposed that the excess plasma membrane formed due to the fusion of secretory vesicles could be accommodated by the formation of invaginations, which are commonly observed at the ultrastructural level (Read and Kalkman, 2003). However, it would be necessary to carry out further analysis to clarify this hypothesis.

5. Conclusions

In summary, we documented the ultrastructure of *P. xanthii* haustoria during the developmental process from incipience to maturity. These findings represent an additional model for investigating the functionality of this fungal "Trojan horse" in maintaining the intimate interaction of powdery mildew species with their host cells. We suggest that the haustorial lobes are the major fungal structure responsible for the exchange of factors with plant cells, the uptake of nutrients from the extrahaustorial matrix, and nutrient delivery to the haustorial body, which would act as a "processing machine". Based on our findings and previous results obtained for other powdery mildew species, we propose a model of vesicular trafficking in *P. xanthii* haustoria in which the majority of secretory and endocytic vesicles are localized in the haustorial lobes (Fig. 9). The endocytic vesicles containing nutrients and RNA might reach the haustorial body vacuoles or might fuse with putative endosomes, resulting in the formation of MVBs due to the invagination of endosomal membranes. Many MVBs serve as transport vehicles for proteins that must be degraded in lysosomes, and other MVBs may merge with the haustorial lobe plasma membrane to deliver small vesicles and exosomes into the EHMx. These putative exosomes might release enzymes, microRNA, mRNA and effectors into the plant cytoplasm through fusion with the EHM.

Acknowledgments

We would like to thank David Navas for help and guidance in the confocal scanning laser microscope. This study was supported by a grant from the Plan Nacional de I+D+I of the former Ministerio de Ciencia e Innovación, Spain (AGL2010-21848-C02-01), co-financed by FEDER funds (European Union). JMC is the recipient of a FPI fellowship from Ministerio de Economía y Competitividad (Spain), and DR is funded by Ramón y Cajal program (RyC-2011-080605) from Ministerio de Economía y Competitividad (Spain).

Appendix A. Supplementary material

Supplementary data associated with this article can be found, in the online version, at http://dx.doi.org/10.1016/j.fgb.2014.08.006.

References

Agrios, G.N., 2005. Plant Pathology, 5th ed. Elsevier, Amsterdam.

Álvarez, B., Torés, J.A., 1997. Cultivo in vitro de *Sphaerotheca fuliginea* (Schlecht. ex. Fr.), efecto de diferentes fuentes de carbón sobre su desarrollo. Bol. San. Veg. Plagas 23, 283–288.

An, Q. et al., 2006. Multivesicular bodies participate in a cell wall-associated defense response in barley leaves attacked by the pathogenic powdery mildew fungus. Cell. Microbiol. 8, 1009–1019.

Bindschedler, L. et al., 2009. In planta proteomics and proteogenomics of the biotrophic barley fungal pathogen *Blumeria graminis* f.sp. *hordei*. Mol. Cell. Proteomics 8, 2368–2381.

Bindschedler, L.V. et al., 2011. Proteogenomics and *in silico* structural and functional annotation of the barley powdery mildew *Blumeria graminis* f.sp. *hordei*. Methods 54, 432–441.

Bolte, S. et al., 2004. FM-dyes as experimental probes for dissecting vesicle trafficking in living plant cells. J. Microsc.-Oxford 214, 159–173.

Both, M. et al., 2005a. Gene expression profiles of *Blumeria graminis* indicate dynamics changes to primary metabolism during development of an obligate biotrophic pathogen. Plant Cell 17, 2107–2122.

Both, M. et al., 2005b. Transcript profiles of *Blumeria graminis* development during infection reveal a cluster of genes that are potential virulence determinants. Mol. Plant-Microbe Interact. 18, 125–133.

Carver, T.L.W. et al., 1999. Release and visualization of the extracellular matrix of conidia of *Blumeria graminis*. Mycol. Res. 103, 547–560.

Cheng, H. et al., 2012. Molecular cloning and expression analysis of CmMlo1 in melon. Mol. Biol. Rep. 39, 1903–1907.

Cohen, Y. et al., 1990. Ultrastructure, autofluorescence, callose deposition and lignification in susceptible and resistant muskmelon leaves infected with the powdery mildew fungus *Sphaerotheca fuligine*. Physiol. Mol. Plant Pathol. 36, 191–204.

del Pino, D. et al., 2002. Occurrence of races and pathotypes of cucurbit powdery mildew in southeastern Spain. Phytoparasitica 30, 459–466.

Eggert, D. et al., 2014. Nanoscale glucan polymer network causes pathogen resistance. Sci. Rep. 4, 4159.

Eichman, R., Hückelhoven, R., 2008. Accommodation powdery mildew fungi in intact plant cells. J. Plant Physiol. 165, 5–18.

Ellinger, D. et al., 2013. Elevated early callose deposition results in complete penetration resistance to powdery mildew in Arabidopsis. Plant Physiol. 161, 1433–1444.

Fernandez-Ortuño, D. et al., 2006. Occurrence and distribution of resistance to QoI fungicides in populations of *Podosphaera fusca* in south central Spain. Eur. J. Plant Pathol. 115, 215–222.

Fischer-Parton, S. et al., 2000. Confocal microscopy of FM4-64 as a tool for analysing endocytosis and vesicle trafficking in living fungal hyphae. J. Microsc. 198, 246–259.

Fofana, B. et al., 2005. Suppression of induced resistance in cucumber through disruption of the flavonoid pathway. Phytopathology 95, 114–123.

Fotopoulos, V. et al., 2003. The monosaccharide transporter gene, *AtSTP4*, and the cell-wall invertase, *Atβfruct1*, are induced in arabidopsis during infection with the fungal biotroph *Erysiphe cichoracearum*. Plant Physiol. 132, 821–829.

Gil, F., Gay, J.L., 1977. Ultrastructural and physiological properties of the host interfacial components of haustoria of *Erysiphe pisi in vivo* and *in vitro*. Physiol. Plant Pathol. 10, 1–12.

Godfrey, D. et al., 2009. A proteomics study of barley powdery mildew haustoria. Proteomics 9, 3222–3232.

Grouffaud, S. et al., 2010. Towards an understanding on how RxLR-effector proteins are translocated from oomycetes into host cells. Fungal Biol. Rev. 24, 27–36.

Hacquard, S. et al., 2013. Mosaic genome structure of the barley powdery mildew pathogen and conservation of transcriptional programs in divergent hosts. Proc. Natl. Acad. Sci. USA 110, E2219–E2228.

Hahn, M., Mendgen, K., 1997. Characterization of in planta-induced rust genes isolated from a haustorium-specific cDNA library. Mol. Plant-Microbe Interact. 10, 427–437.

Koeck, M. et al., 2011. The role of effectors of biotrophic and hemibiotrophic fungi in infection. Cell. Microbiol. 13, 1849–1857.

Koh, S. et al., 2005. *Arabidopsis thaliana* subcellular responses to compatible *Erysiphe cichoracearum* infections. Plant J. 44, 516–529.

Kuzuya, M. et al., 2006. Powdery mildew (*Podosphaera xanthii*) resistance in melon is categorized in two types based on inhibition of the infection processes. J. Exp. Bot. 57, 2093–2100.

Lewis, M.W. et al., 2009. Uptake of the fluorescent probe FM4-64 by hyphae and haemolymph-derived *in vivo* hyphal bodies of the entomopathogenic fungus *Beauveria bassiana*. Microbiology 155, 3110–3120.

Lipka, V., Panstruga, R., 2005. Dynamic cellular responses in plant-microbe interactions. Curr. Opin. Plant Biol. 8, 625–631.

Lu, Y.J. et al., 2012. Patterns of plant subcellular responses to successful oomycete infections reveal differences in host cell reprogramming and endocytic trafficking. Cell. Microbiol. 14, 682–697.

Mackie, A.J. et al., 1993. Glycoproteins recognized by monoclonal antibodies UB7, UB8 and UB10 are expressed early in the development of pea powdery mildew haustoria. Physiol. Mol. Plant Pathol. 43, 135–146.

Manners, J.M., Gay, J.L., 1977. The morphology of haustorial complexes isolated from apple, barley, beet and vine infected with powdery mildews. Physiol. Plant Pathol. 11, 261–266.

Meyer, D. et al., 2009. Extracellular transport and integration of plant secretory proteins into pathogen-induced cell wall compartments. Plant J. 57, 986–999.

Miazzi, M. et al., 2011. Variation in *Podosphaera xanthii* on cucurbits in Southern Italy. J. Phytopathol. 159, 538–545.

Micali, C. et al., 2011. Biogenesis of a specialized plant-fungal interface during host cell internalization of *Golovinomyces orontii* haustoria. Cell. Microbiol. 13, 210–226.

Miklis, M. et al., 2007. Barley MLO modulates actin-dependent and actin-independent antifungal defense pathways at the cell periphery. Plant Physiol. 144, 1132–1143.

Naumann, M. et al., 2013. Differences in early callose deposition during adapted and non-adapted powdery mildew infection of resistant *Arabidopsis* lines. Plant Signal. Behav. 8, e24408.

Olesen, K.L. et al., 2003. Fungal suppression of resistance against inappropriate *Blumeria graminis forma especiales* in barley, oat and wheat. Physiol. Mol. Plant Pathol. 62, 37–50.

Opalski, K.S. et al., 2005. The receptor-like MLO protein and the RAC/ROP family G-protein RACB modulate actin reorganization in barley attacked by the biotrophic powdery mildew fungus *Blumeria graminis* f. sp *hordei*. Plant J. 41, 291–303.

Panstruga, R., 2003. Establishing compatibility plants and obligate biotrophic pathogens. Curr. Opin. Plant Biol. 6, 320–326.

Pérez-García, A. et al., 2009. The powdery mildew fungus *Podosphaerafusca* (synonym *Podosphaera xanthii*), a constant threat to cucurbits. Mol. Plant Pathol. 10, 153–160.

Pliego, C. et al., 2013. Host-induced gene silencing in barley powdery mildew reveals a class of ribonuclease-like effectors. Mol. Plant Microbe Interact. 26, 633–642.

Puthoff, D.P. et al., 2008. Analysis of expressed sequence tags from *Uromyces appendiculatus* hyphae and haustoria and their comparison to sequence from other rust fungi. Phytopathology 98, 1126–1135.

Rafiqi, M. et al., 2010. Internalization of flax rust avirulence proteins into flax and tobacco cells can occur in the absence of the pathogen. Plant Cell 22, 2017–2032.

Read, N.D., Kalkman, E.R., 2003. Does endocytosis occur in fungal hyphae? Fungal Genet. Biol. 39, 199–203.

Rivera, M.E. et al., 2002. Differential expression of *β*-1,3-glucanase in susceptible and resistant melon cultivars in response to infection by *Sphaerotheca fusca*. Physiol. Mol. Plant Pathol. 61, 257–265.

Rodrigues, M.L. et al., 2008. Vesicular *trans-cell* wall transport in fungi: a mechanism for the delivery of virulence-associated macromolecules? Lipid Insights 2, 27–40.

Romero, D. et al., 2008. Comparative histochemical analyses of oxidative burst and cell wall reinforcement in compatible and incompatible melon-powdery mildew (*Podosphaera fusca*) interactions. J. Physiol. 165, 1895–1905.

Schorey, J.S., Bhatnagar, S., 2008. Exosome function: from tumor immunology to pathogen biology. Traffic 9, 871–881.

Schultheiss, H. et al., 2008. Barley RIC171 interacts with RACB *in planta* and supports entry of powdery mildew fungus. Cell. Microbiol. 10, 1815–1826.

Sedlářová, M. et al., 2009. Histological aspects of *Cucumis melo* PI 313970 resistance to *Podosphaera xanthii* and *Golovinomyces cichoracearum*. J. Plant Dis. Protect. 116, 169–176.

Spanu, P.D. et al., 2010. Genome expansion and gene loss in powdery mildew fungi reveal tradeoffs in extreme parasitism. Science 330, 1543–1546.

Théry, C., 2011. Exosomes: secreted vesicles and intercellular communications. F1000. Biol. Rep. 3, 15.

Torralba, S., Heath, I.B., 2002. Analysis of three separate probes suggests the absence of endocytosis in *Neurospora crassa* hyphae. Fungal Genet. Biol. 37, 221–232.

Valadi, H. et al., 2007. Exosome-mediated transfer of mRNAs and microRNAs is a novel mechanism of genetic exchange between cells. Nat. Cell Biol. 9, 654–659.

Voegele, R.T., Mendgen, K., 2003. Rust haustoria: nutrient uptake and beyond. New Phytol. 159, 93–100.

Wang, W. et al., 2009. Specific targeting of the *Arabidopsis* resistance protein RPW8.2 to the interfacial membrane encasing the fungal haustorium renders broad-spectrum resistance to powdery mildew. Plant Cell 21, 2898–2913.

Wen, Y. et al., 2011. Identification and utilization of a sow thistle powdery mildew as a poorly adapted pathogen to dissect post-invasion non-host resistance mechanisms in *Arabidopsis*. J. Exp. Bot. 62, 2117–2129.

Weßling, R. et al., 2012. Transcriptome analysis of enriched *Golovinomyces orontii* haustoria by deep 454 pyrosequencing. Fungal Genet. Biol. 49, 470–482.